Methods and Applications

Establishment and Application of a Radiation Dose Rate Model for Nuclear Medicine Examinees

Yuehua Hu[1,&]; Xinyu He[2,&]; Wenjia Zhao[1]; Lixin Ding[3]; Meiying You[1]; Zihan Li[1]; Xinyu Liu[1]; Miaomiao Wang[1]; Siyi Chen[4]; Ziwei Lu[5]; Lei Qu[6]; Kuke Ding[7]; Li Zhang[7,#]; Qiuxian Fu[8,#]

ABSTRACT

Introduction: Traditional methods for determining radiation dose in nuclear medicine include the Monte Carlo method, the discrete ordinate method, and the point kernel integration method. This study presents a new mathematical model for predicting the radiation dose rate in the vicinity of nuclear medicine patients.

Methods: A new algorithm was created by combining the physical model of "cylinder superposition" of the human body with integral analysis to assess the radiation dose rate in the vicinity of nuclear medicine patients.

Results: The model accurately predicted radiation dose rates within distances of 0.1–3.0 m, with a deviation of less than 11% compared to observed rates. The model demonstrated greater accuracy at shorter distances from the radiation source, with a deviation of only 1.55% from observed values at 0.1 m.

Discussion: The model proposed in this study effectively represents the spatial and temporal distribution of the radiation field around nuclear medicine patients and demonstrates good agreement with actual measurements. This model has the potential to serve as a radiation dose rate alert system in hospital environments.

During positron emission tomography/computed tomography (PET/CT) testing, it is crucial to administer radioactive isotopes. The γ radiation from these isotopes poses risks to nearby individuals, including medical staff, patients' families, and other nuclear medicine patients. Therefore, assessing the dose rate is essential for ensuring the safety of these individuals in close proximity.

Various methods are employed to calculate dose rates in radiation scenarios, including the Monte Carlo method, the discrete ordinate method, and the point kernel integration method. Each method has its strengths and limitations. The Monte Carlo method uses probability and statistics but can be computationally slow and occasionally unsolvable (*1*). The discrete ordinate method offers fast calculations but struggles with complexity in large systems. The point kernel integration method uses a uniform grid for radiation sources but lacks real-time capabilities (*2*–*4*). To address these limitations, the "cylinder integration" method was developed to create a spatial-temporal model for radiation dose rates around nuclear medicine patients (*5*), offering a simplified and innovative approach to calculations.

METHODS

Upon injection, ^{18}F-FDG rapidly dispersed throughout the body, achieving nearly complete distribution across organs within about 30 seconds (*6*). Gray-scale physical models were generated for each organ, correlating with their respective gray-scale values (Figure 1). Post-injection, gray-scale imaging was calibrated at three time points: 350–360 seconds (A1), 1,770–1,800 seconds (B1), and 3,480–3,600 seconds (C1), with radionuclide activity represented in charts A2, B2, and C2. For example, the radioactivity levels in different body regions at time points B2 and C2 can be illustrated by assigning values a_1 to the head, a_2 to the trunk, a_3 to the heart, a_4 to the bladder, and a_5 to the legs. Detailed methodology for determining these values is provided in Supplementary Materials (available at https://weekly.chinacdc.cn/).

The methodology for calculating the radiation dose rate around organs that are symmetric along a common axis in the body is provided in the Supplementary Materials. To assess the radiation dose distribution from organs such as the heart, tumor, and legs, which are not aligned with the Z-axis of the cylinder, a translation technique was utilized to align them with

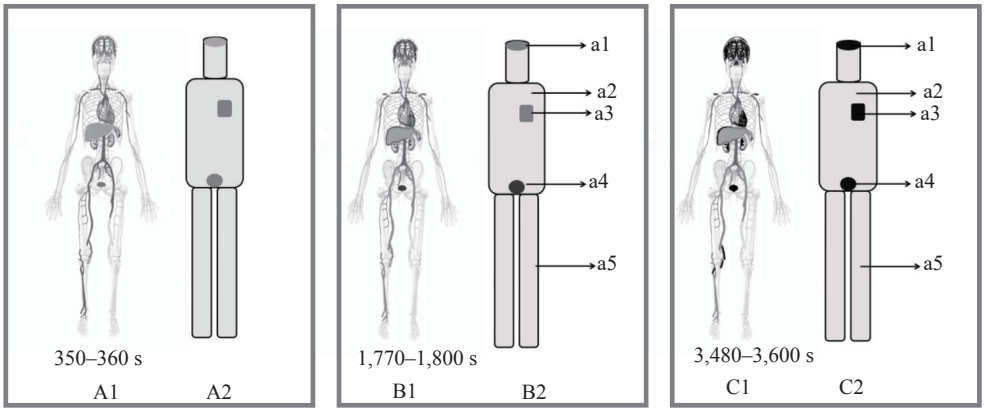

FIGURE 1. Schematic diagram of the grayscale values and corresponding specific activity of PET/CT or PET images. (A1) Gamma-ray imaging of the human body 350 to 360 seconds after radiopharmaceuticals are injected into the patient; (A2) Grayscale image of its corresponding organ; (B1) Gamma-ray imaging of the human body between 1,770 and 1,800 seconds after radiopharmaceutical injection into the patient; (B2) Grayscale image of its corresponding organ; (C1) Gamma-ray imaging of the human body 3,480 to 3,600 seconds after the injection of radiopharma into the patient; (C2) Grayscale image of its corresponding organ.
Abbreviation: PET/CT=positron emission tomography/computed tomography.

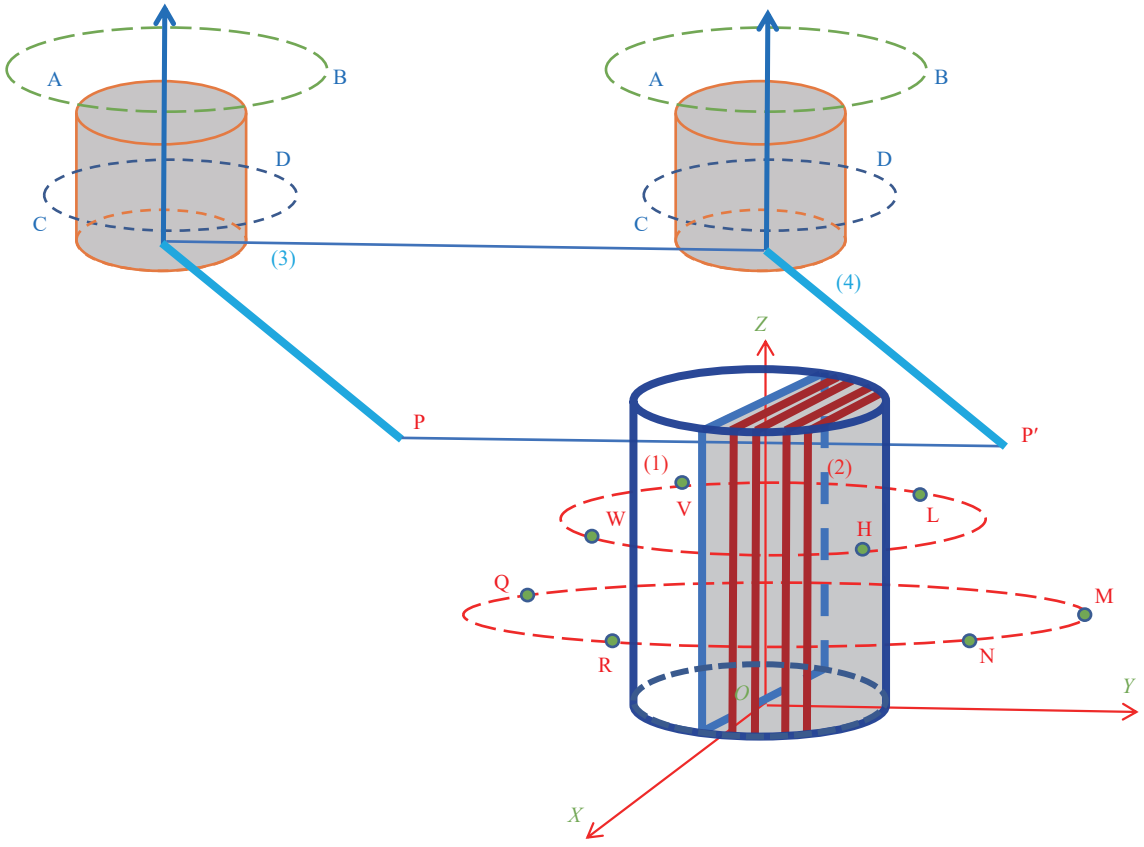

FIGURE 2. Schematic diagram illustrating the calculation of radiation dose rates around organs with non-axisymmetric axes.
Note: In the same way that P is translated to P ', (3) is translated to (4), coaxial with (1) and (2) below.
The four points W, V, H and L mean that the four points are coaxial and on the same plane at the same height, so the radiation dose rate is the same; The four points, N, M, Q, R, are coaxial and on the same plane at the same height, so the radiation dose rate is the same.

the Z-axis using the equation OP=O′ P′ (Figure 2). This method ensured that the radiation dose rates at points P and P′ were equal. Additional information on the derivation process is available in the

Supplementary Materials.

The method used for calculation assumes a uniform distribution of radioactive activity in the body, which may not always hold true. To improve accuracy, we introduced a "radiation dose rate correction factor" (ω) by comparing measured radiation dose rates near the body. ω was determined as the average of theoretical and observed dose rates at different distances. Despite metabolic differences in radioactive pharmaceuticals, the corrected relative error remained below 11%, indicating the general applicability of the correction factor ω.

The patient was injected with 127.4 MBq of ^{18}F-FDG imaging agent through the median elbow vein at a hospital. The imaging agent, supplied by Beijing Atomic High Tech Co., Ltd., had a radiochemical purity of over 95%. Portable model 6,150 by Automes from Germany γ Peripheral dose equivalent rate instrument was used to measure the dose equivalent rate of radiation. Measurements were taken while the patient stood with hands naturally hanging down, the detector placed at the center of the patient's chest facing forward. Measurements began 99 minutes post-injection, with distances ranging from 0.1 m to 3.0 m from the patient's body surface. Each measurement, lasting 30 seconds, was repeated three times, recorded after stabilization, and averaged after background dose subtraction.

RESULTS

The method used to calculate the spatiotemporal distribution of radiation dose around a single cylindrical model can be found in the Supplementary Materials. Different body parts such as the head, trunk, legs, heart, bladder, and tumor were represented by cylinders in the mathematical model to estimate the radiation dose rate. The spatiotemporal radiation dose distribution around an individual was determined using the superposition method of coaxial and non-coaxial cylinder values.

To account for variations in height, weight, stance, and timing of radiopharmaceutical administration among subjects, standardization within a consistent coordinate system was essential, achieved through our computational model. The model's unique aspect is the use of position translation to achieve a uniform spatiotemporal distribution of radiation dose rates. We harmonized horizontal discrepancies by aligning the subjects' positions using horizontal translation (Figure 3). For individuals with different leg lengths, vertical height translation aligned their origin within the coordinate system, enabling precise dose rate comparisons. Additionally, we synchronized temporal variations in radiopharmaceutical administration by adjusting the starting times in the temporal parameter t, ensuring consistent dose rate calculation regardless of injection schedule differences.

Using the "cylinder" model and its associated algorithm, we estimated the radiation dose rate for the subject. We then compared this estimate to the actual measured data, allowing us to ascertain the deviation and calculate the mean discrepancy, denoted as ω. Table 1 presents the relative differences between the

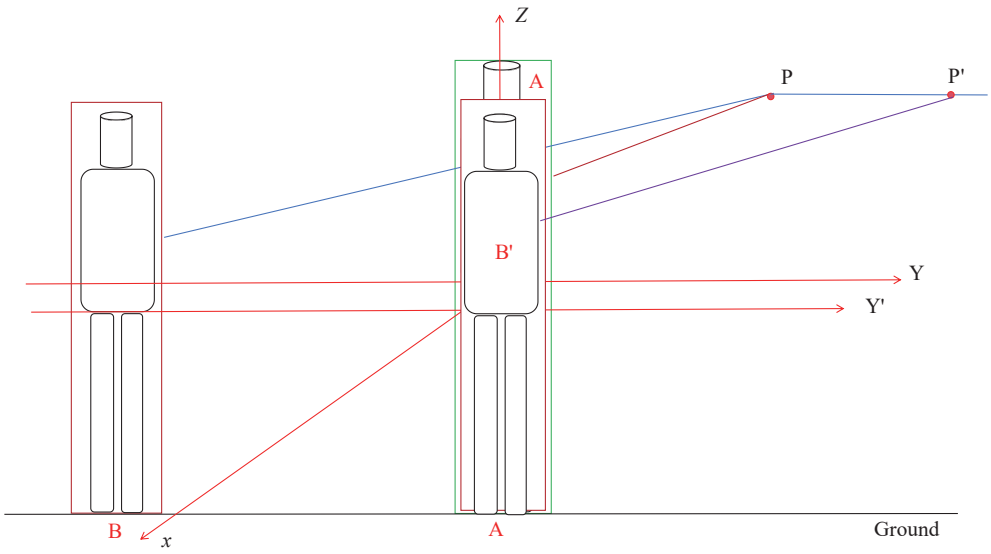

FIGURE 3. The standing positions of subjects A and B within the same space.

TABLE 1. Comparison of calculated and measured radiation dose rates.

Distance between the point and the body surface (m)	Theoretical rate (μGy·h $^{-1}$)	Measured rate (μGy·h $^{-1}$)	Difference (μGy·h $^{-1}$)	ω (μGy·h $^{-1}$)	Uncorrected relative error (%)	Corrected relative error (%)
0.1	242.48	238.78	3.70		1.55	1.81
0.5	44.56	41.02	3.54		8.63	10.16
1.0	14.50	16.65	−2.15	0.626	−12.91	−9.15
2.0	4.14	5.33	−1.19		−22.33	−10.58
3.0	1.92	2.69	−0.77		−28.62	−5.35

theoretical and measured dose rates. After applying the model's corrections for distances spanning from 0.1 to 3.0 meters, we found that the estimated dose rates consistently correlated with the measured values, exhibiting variances of less than 11%.

DISCUSSION

Using a sophisticated human body model based on cylindrical elements, we have developed an integral solution that evolves from "point" to "line" and then to "surface" infinitesimals, allowing us to accurately compute the spatiotemporal distribution of radiation dose rates in the vicinity of nuclear medicine patients. The strength of this algorithm is rooted in its sound scientific principles and meticulous mathematical framework. Importantly, the model moves beyond the overly simplistic "point" or "line" representations of the human body and incorporates a more complex, layered cylindrical approach. This enhancement significantly improves the fidelity of simulations across various clinical situations, whether assessing radiation dose distribution around a single patient or multiple patients located on the same plane following radiopharmaceutical administration. The flexibility of the algorithm confirms its wide-ranging clinical utility. Through comparative calculations and validations, we have demonstrated that the estimated radiation dose rates at distances ranging from 0.1 to 3.0 meters are consistent with actual measurements. While some deviations exceeded 5 percent, they remained below the acceptable dose variation threshold of 15 percent, affirming the algorithm's suitability for clinical use. These results validate that the integration of a comprehensive computational strategy with a cylindrical superposition model of the human body considerably improves the accuracy of predicted dose rate distributions, thereby more closely reflecting the real radiation exposure levels around patients.

This study is subject to some limitations. First, the necessity of computational software development is crucial to expedite the application process due to the complex calculations involved. Second, there is a discrepancy of 10.58% between measured and calculated values, attributed to the human body being simplified as a "cylinder". To reduce this error, measurements should be taken with a human body model utilizing "cylinder superposition". Third, it is essential to increase the radiation dose rate measurements around more participants to obtain an accurate correction factor for the radiation dose rate (ω).

Conflicts of interest: No conflicts of interest.

Acknowledgements: Shixi Zheng, Shuyuan Liu, Ziwei Lu, and Lei Qu for their contributions in preparing the figures.

Funding: Supported by the National Natural Science Foundation of China (grant nos. 31770907, 31640022 and 31170806), and the Beijing Natural Science Foundation (grant no. 7172146).

doi: 10.46234/ccdcw2024.108

[#] Corresponding authors: Li Zhang, Zhangli@chinacdc.cn; Qiuxian Fu, fuqiuxian51@163.com.

[1] Office of Epidemiology, Chinese Center for Disease Control and Prevention, Beijing, China; [2] Department of Oncology, Central Hospital Affiliated to Shandong First Medical University, Jinan City, Shandong Province, China; [3] National Institute for Radiological Protection, Chinese Center for Disease Control and Prevention, Beijing, China; [4] National Center for Chronic and Noncommunicable Disease Control and Prevention, Chinese Center for Disease Control and Prevention, Beijing, China; [5] Laboratory Animal Center, Chinese Center for Disease Control and Prevention, Beijing, China; [6] National Institute of Parasitic Diseases, Chinese Center for Disease Control and Prevention, Shanghai, China; [7] Office of Public Health Management, Chinese Center for Disease Control and Prevention, Beijing, China; [8] Hainan Medical University, Haikou City, Hainan Province, China.
[&] Joint first authors.

Submitted: January 05, 2024; Accepted: March 05, 2024

REFERENCES

1. Huang Y, Liu HK. Development and application of graphics processor units-based Monte Carlo simulation in radiation dose calculation. Chin J Med Phys 2017;34(10):973 – 4. https://doi.org/10.3969/j.issn.1005-202X.2017.10.001. (In Chinese).
2. Ohga Y, Fukuda M, Shibata K, Kawakami T, Matsuzaki T. A system for the calculation and visualisation of radiation field for maintenance support in nuclear power plants. Radiat Prot Dosimetry 2005;116(1-4 Pt

2):592 – 6. http://dx.doi.org/10.1093/rpd/nci014.
3. Subbaiah KV, Sarangapani R. GUI2QAD-3D: a graphical interface program for QAD-CGPIC program. Ann Nuclear Energy 2006;33(1):22 – 9. https://doi.org/10.1016/j.anucene.2005.07.009.
4. Ingersoll DT. User's manual for PUTZ: a point-kernel photon shielding code. Oak Ridge National Lab. 1986. https://inis.iaea.org/search/search.aspx?orig_q=RN%3A18001366. [2023-12-19].
5. China State Bureau of Technical Supervision. GB/T 10000-1988 Human dimensions of Chinese adults. Beijing: Standards Press of China, 1988. https://openstd.samr.gov.cn/bzgk/gb/newGbInfo?hcno=A78583489235BF9BF9EE253E74DC76B9. (In Chinese).
6. Tan H, Qi C, Cao YY, Cai DJ, Mao WJ, Yu HJ, et al. Ultralow-dose [^{18}F]FDG PET/CT imaging: demonstration of feasibility in dynamic and static images. Eur Radiol 2023;33(7):5017 – 27. https://doi.org/10.1007/s00330-023-09389-3.

SUPPLEMENTARY MATERIAL

The Establishment of Physical Model in A "Cylinder Superposition"

According to the physical model known as "cylinder superposition," the following relationships are established.

$$\left(\pi \mathrm{R}_1^2 h_1 + \pi \mathrm{R}_2^2 h_2 + 2\pi \mathrm{R}_3^2 h_3\right)\rho = \mathrm{Mg} \tag{1}$$

$$h_1 + h_2 + h_3 = \mathrm{H} \tag{2}$$

$$\rho = \frac{\mathrm{Mg}}{\mathrm{V}} \tag{3}$$

The Mathematical Model Corresponding to the Gray Value of Image and the Specific Activity of the Corresponding Part

Assuming the patient's weight is represented by Mg (kg), height by H (m), actual body volume by V (m^3) obtained through full water immersion, head height by h_1 (m), torso height by h_2 (m), leg height by h_3 (m), head radius by R_1 (m), torso radius by R_2 (m), leg radius by R_3 (m), and average human body density by ρ (kg/m^3).

It is essential to understand the relationship between the gray scale values of images and the activity of radionuclides at their respective sites. To establish this, two time points post-radiopharmaceutical injection, denoted as t_1 and t_2, were designated. PET-CT or PET images from these time intervals (1,770–1,800 seconds, 3,480–3,600 seconds) were chosen to represent each period (Figure 1). Assuming the patient does not void urine during the scanning, the following two equations can be deduced:

$$\begin{aligned} D_0 e^{-\lambda_1 t_1} &= \pi \mathrm{k} \mathrm{R}_1^2 h_1 a_{1t_1} + \pi \mathrm{k} \mathrm{R}_2^2 h_2 a_{2t_1} + \pi k R_4^2 h_4 \left(a_{3t_1} - a_{2t_1}\right) \\ &\quad + \pi k R_5^2 h_5 \left(a_{4t_1} - a_{2t_1}\right) + 2\pi k R_3^2 h_3 a_{5t_1} \end{aligned} \tag{4}$$

$$\begin{aligned} D_0 e^{-\lambda_1 t_2} &= \pi \mathrm{k} \mathrm{R}_1^2 h_1 a_{1t_2} + \pi \mathrm{k} \mathrm{R}_2^2 h_2 a_{2t_2} + \pi k R_4^2 h_4 \left(a_{3t_2} - a_{2t_2}\right) \\ &\quad + \pi k R_5^2 h_5 \left(a_{4t_2} - a_{2t_2}\right) + 2\pi k R_3^2 h_3 a_{5t_2} \end{aligned} \tag{5}$$

In the equations:

D_0 represents the initial activity value of ^{18}F-FDG injected into the body.

k is the scale factor between the radionuclide activity value and the gray-scale value of the image;

λ_1 represents the radioactive decay rate of ^{18}F-FDG, while λ_2 indicates the variation coefficient of metabolism in a specific organ, excluding the bladder.

h_4 represents the height of the "cylinder" corresponding to the heart; h_5 represents the height of the "cylinder" corresponding to the bladder;

R_4 represents the radius of the heart "cylinder" and R_5 represents the radius of the bladder "cylinder";

$a_{1t_1}, a_{2t_1}, a_{3t_1}, a_{4t_1}, a_{5t_1}$ are the radionuclide activity values in the head, trunk, heart, bladder, and legs, measured at 1,770–1,800 seconds post-injection of the radiopharmaceutical;

$a_{1t_2}, a_{2t_2}, a_{3t_2}, a_{4t_2}, a_{5t_2}$ are the radionuclide activity values in the head, trunk, heart, bladder, and legs, measured at 3,480–3,600 seconds post-injection of the radiopharmaceutical.

The Calculation of the Spatial and Temporal Distribution of Radiation Dose Rates Around a Single "Cylinder Model"

It is essential to apply the integral method to calculate the infinitesimal solutions of points, lines, and surfaces of cylinders.

(i) Integral solutions for making the point infinitesimal: The research focuses on determining radiation dose distributions for cylindrical structures using the integration of infinitesimal points, lines, and surfaces within a human body model. This involves employing the concept of "cylinder superposition" to calculate radiation dose rates from point sources at varying distances, such as the "infinitesimal" MN on a linear radioactive source within the EF line segment (Figure 1).

According to the isotropic point source γ dose rate formula $\left(X_0 = \frac{Q\Gamma}{R_{dp}^2}\right)$(*1*), for a specific monoenergetic gamma

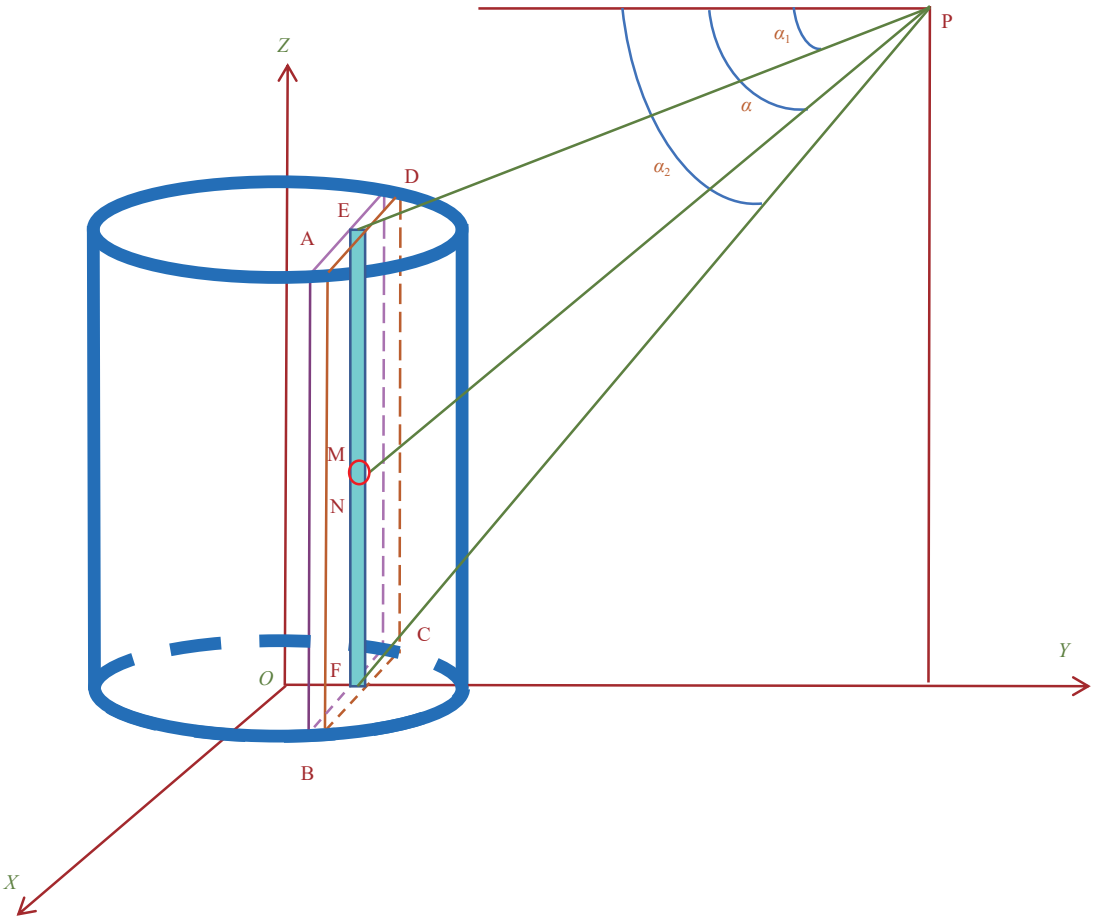

SUPPLEMENTARY FIGURE S1. An “infinitesimal” MN on a “line source” EF.

ray emitted from a particular radioisotope, the Γ-constant used is the differential Γ-constant, represented as Γ_i. The total Γ-constant for the radioisotope, referred to as the Γ-constant, is the cumulative sum of Γ_i, which can be determined as follows:

$$\Gamma = 1.54 \times 10^5 \Sigma_{i-1}^{m} E_i n_i R_i \tag{6}$$

(ii) Integral solutions for making the line infinitesimal: By utilizing the spatial and temporal distribution solution of the radiation dose rate M_{head} surrounding a head cylinder model, we consider the distance between EF and PH as h_F (i.e., the length of FH) (Supplementary Figure S2).

The angle between EF and PF is denoted as θ_1, the angle between the extension of FE and PE is denoted as θ_2, and the angle between FN and NP is denoted as θ. The main integral equation is:

The height of $\bar{EF}$ is assumed to be h,

$$dM_{\text{head}} = \frac{A_{\text{head}}\,\Gamma_\delta}{r^2} dz \tag{7}$$

$$\begin{aligned} \dot{M}_{head} &= \int \frac{A_{head}\Gamma_\delta}{r^2} dz \\ &= \int \frac{D_0 e^{-\lambda t} a_{1t_1}\Gamma_\delta}{r^2} e^{-\lambda t} dz \\ &= \int \frac{D_0 e^{-\lambda t} a_{1t_1}\Gamma_\delta}{\left(\frac{h_F}{\sin\theta}\right)^2} e^{-\lambda t} d\left(-\frac{h_F}{\tan\theta}\right) \\ &= \frac{D_0 a_{1t_1}\Gamma_\delta e^{-\lambda t}}{h_F}(\theta_2 - \theta_1) \end{aligned} \tag{8}$$

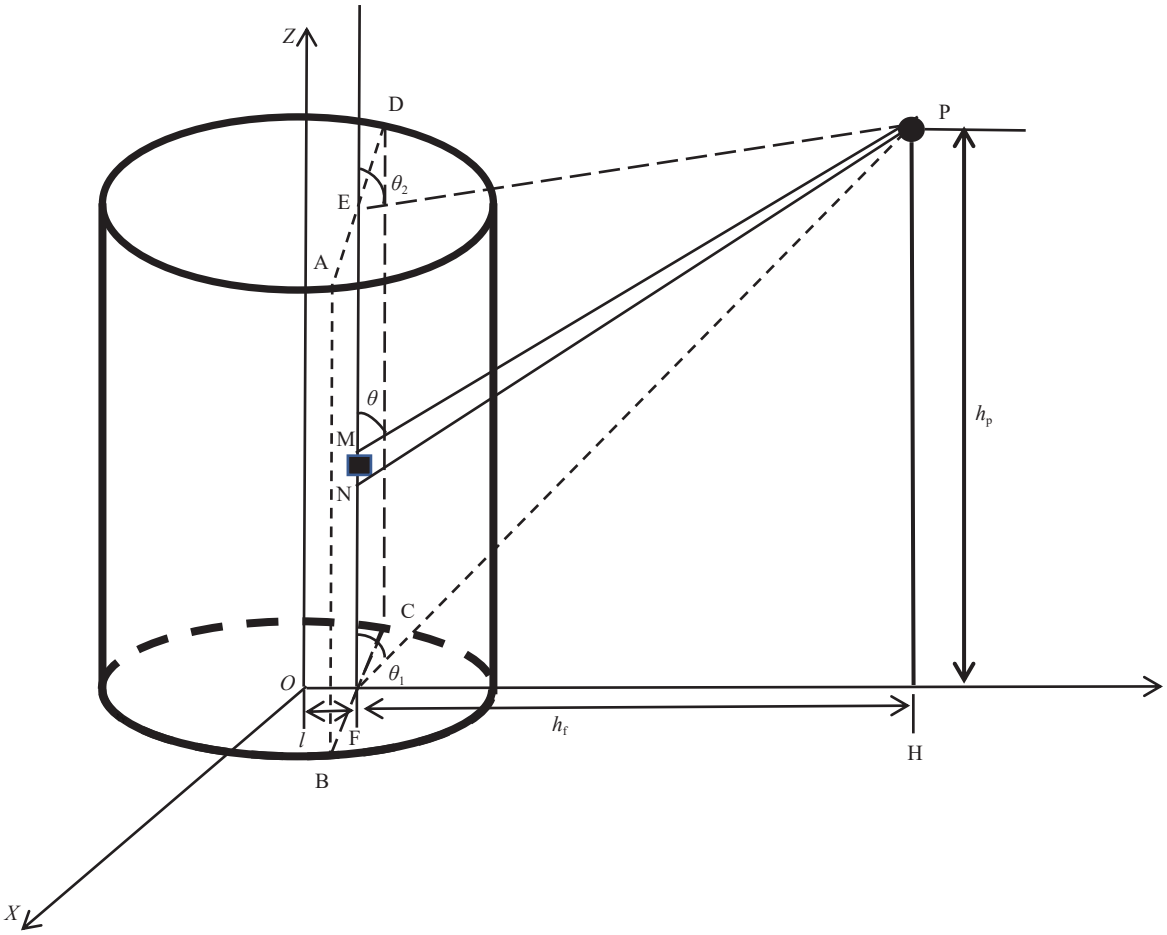

SUPPLEMENTARY FIGURE S2. The "infinitesimal" MN on the head cylinder "line source" EF.

Where D_0, $a_{1_{\delta}}$, r δ, t, and λ are constants, and r represents the distance from an infinitesimally small point to the point P in an external space.

The equation is depicted in Supplementary Figure S3.

$$m^2 = x^2 + H_p^2 \tag{9}$$

Supplementary Figure S4 illustrates the solution for θ 2
when $h_p - h > 0$,

$$\tan\theta_2 = \frac{m_0}{h_p - h} \tag{10}$$

when $h_p - h < 0$, $\tan(180^\circ - \theta_2) = \frac{m_0}{h - h_p}$, then

$$\tan\theta_2 = \frac{m_0}{h_p - h} \tag{11}$$

thus,

$$\theta_2 = \arctan\left(\frac{m_0}{h_p - h}\right) \tag{12}$$

(iii) Integral solutions for infinitesimal surface elements: Based on the aforementioned line integrals, the surface integral ABCD is computed for the infinitesimal line EF (Supplementary Figure S5).

Considering the continued use of the head cylinder model as an example, we computed the vertical surface integral of the head's thin surface (Supplementary Figure S2).

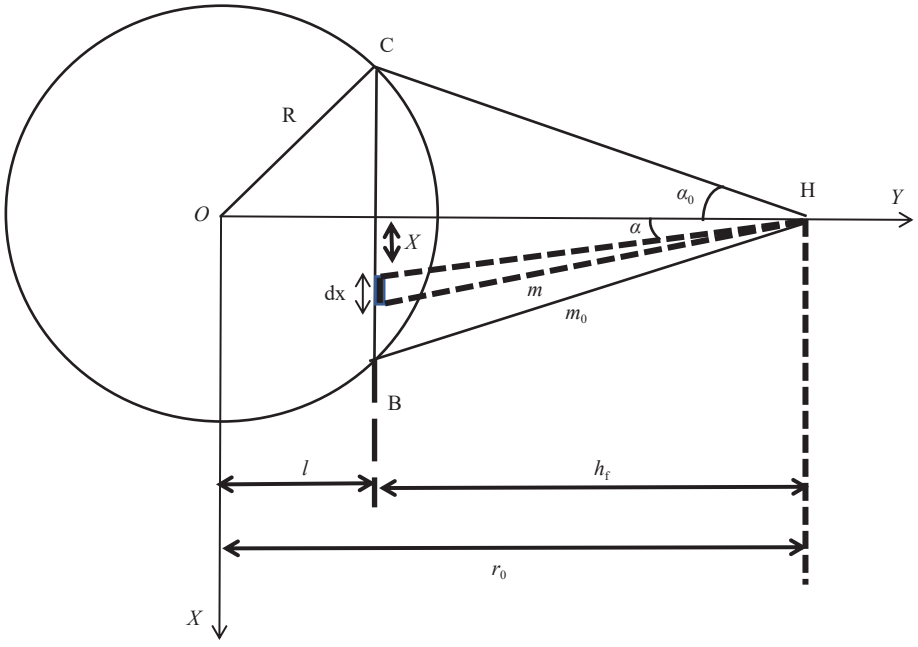

SUPPLEMENTARY FIGURE S3. Bottom view of the head cylinder model.

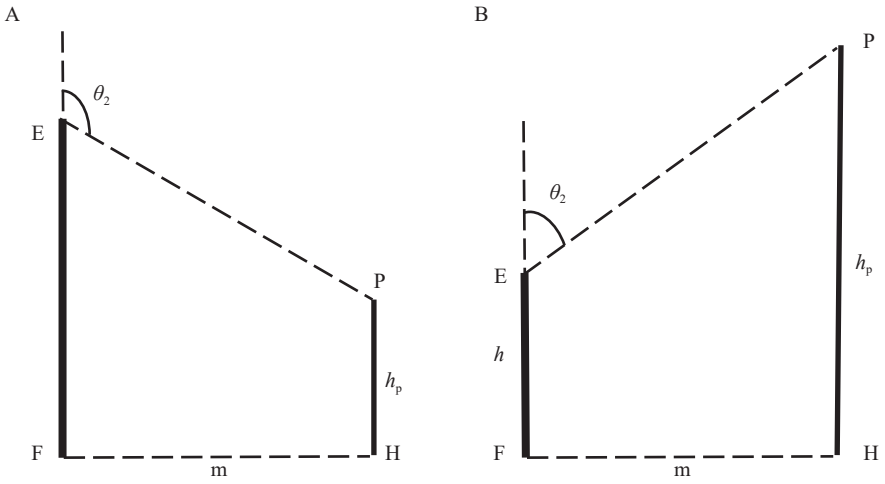

SUPPLEMENTARY FIGURE S4. (A). The relative positions of line segment EF and point P (h_p-h>0). (B) The relative positions of line segment EF and point P (h_p-h<0).

$$
\begin{aligned}
S_{(l)} &= 2\int_0^{\sqrt{R^2-l^2}} \frac{D_0 a_{1t_1} \Gamma_\delta e^{-\lambda t}}{h_F} (\theta_2 - \theta_1)\, dx \\
&= 2\int_0^{\sqrt{R^2-l^2}} \frac{D_0 a_{1t_1} \Gamma_\delta e^{-\lambda t}}{h_F} \left(\arctan\left(\frac{\sqrt{(r_0 - l)^2 + x^2}}{h_p - h} \right) \right. \\
&\quad \left. - \arctan\left(\frac{\sqrt{(r_0 - l)^2 + x^2}}{h_p} \right) \right) dx
\end{aligned} \tag{13}
$$

The volume integral was conducted for the infinitesimal surface ABCD using the surface integral mentioned previously (Supplementary Figure S6).

If the head cylinder model is used as an example, the head volume integral is calculated.

The volume integral of the right half cylinder is calculated as:

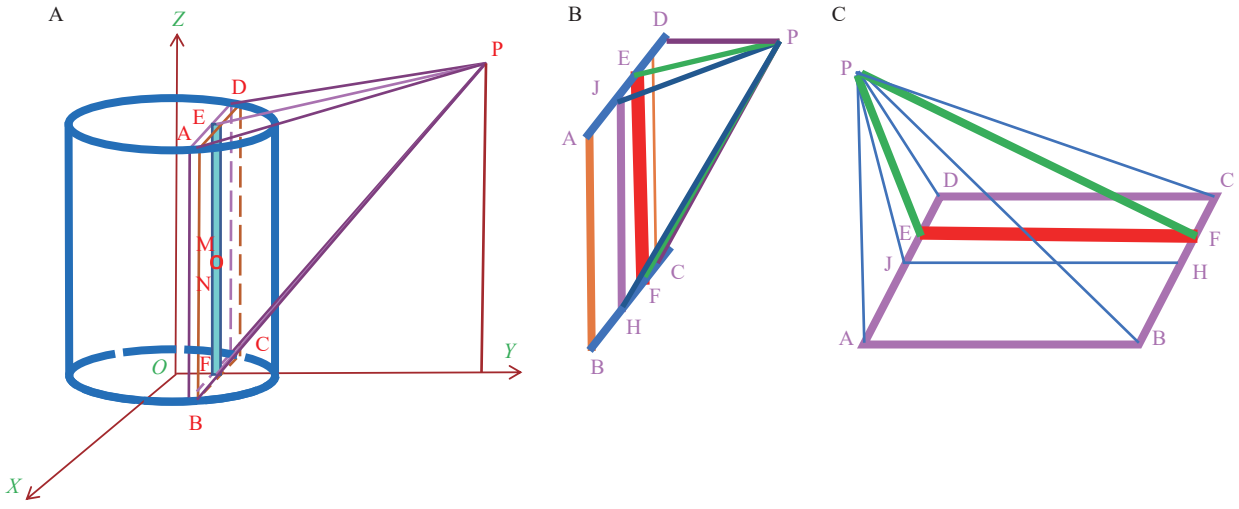

SUPPLEMENTARY FIGURE S5. A surface integral of ABCD (with the line segment EF as infinitesimal).
Note: "A" represents the line infinitesimal diagram, "B" indicates the position of point P relative to the surface ABCD, and "C" illustrates the rotation diagram for "B".

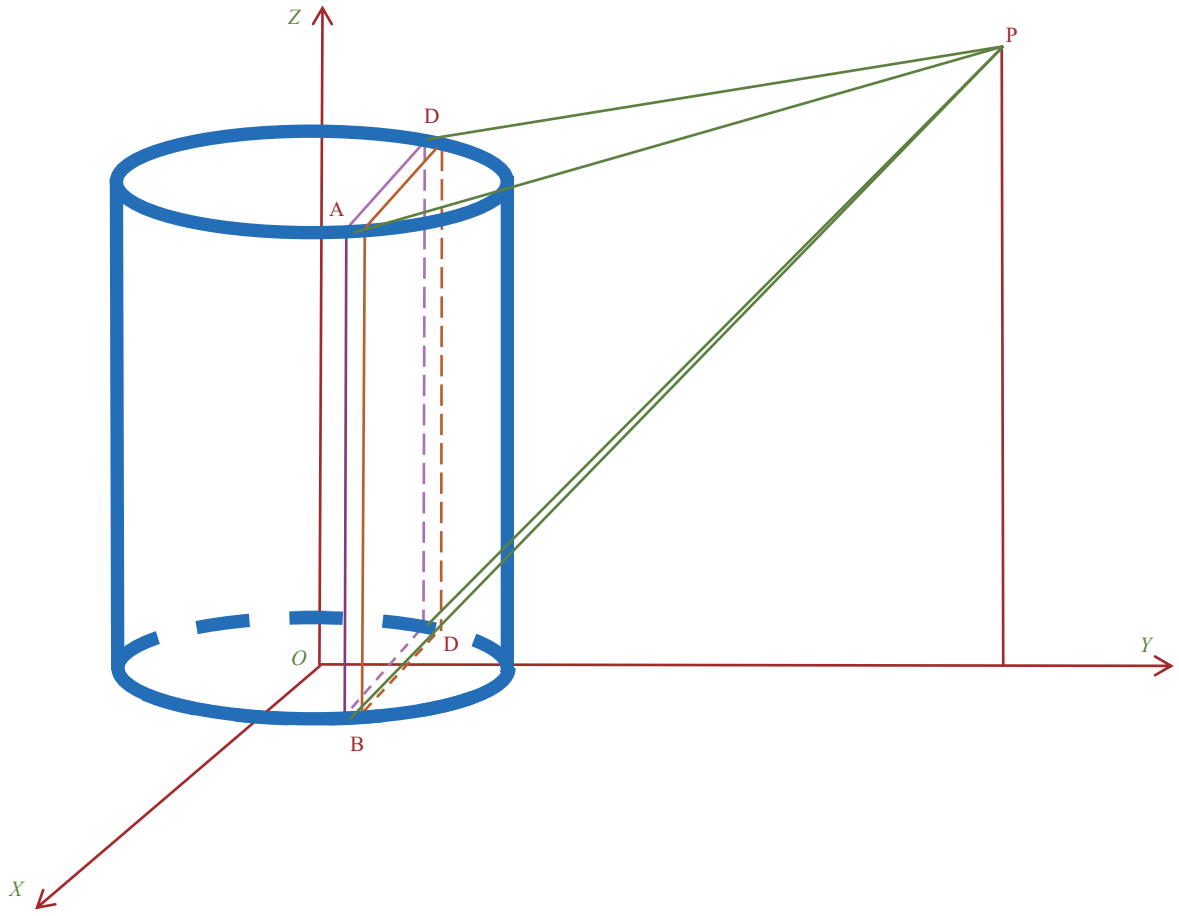

SUPPLEMENTARY FIGURE S6. Volume integral of cylinders with a thin surface ABCD as "infinitesimal".

The line between point D and the center point O forms an angle ϕ with the y-axis and $\angle COQ=\beta$ (Supplementary Figure S7).

Because $x > 0$ and $y > 0$,

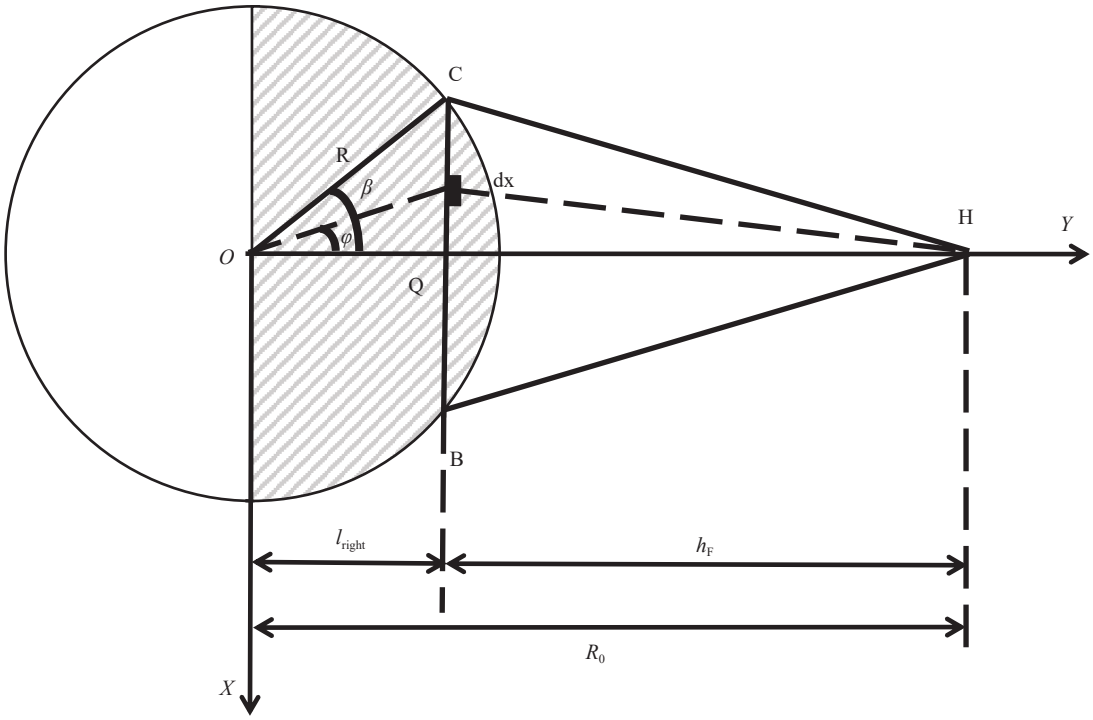

SUPPLEMENTARY FIGURE S7. Bottom view of the right half cylinder model.

$$S_{(l)right} = \int_0^{\beta} \frac{D_0 a_{1t_1} \Gamma_\delta e^{-\lambda t}}{h_F} \left(\arctan\left(\frac{\sqrt{(r_0 - R\cos\beta)^2 + (R\cos\beta\tan\phi)^2}}{h_p - h} \right) - \arctan\left(\frac{\sqrt{(r_0 - R\cos\beta)^2 + (R\cos\beta\tan\phi)^2}}{h_p} \right) \right) \frac{R\cos\beta}{\cos^2\phi} d\phi \tag{14}$$

The radiation dose rate to point P from the right half of the cylinder in the region where y>0 is represented by the variable G_{right}:

$$G_{right} = 2\int_0^{\frac{\pi}{2}} S_{(l)right} R\cos\beta d\beta \tag{15}$$

The volume integral of the left half cylinder was calculated as shown in Supplementary Figure S8.

When x>0, y<0,

$$\begin{aligned} S_{(l)left} &= \int_{\beta}^{\pi} \frac{D_0 a_{1t_1} \Gamma_\delta e^{-\lambda t}}{h_F} \left(\arctan\left(\frac{\sqrt{(r_0 + l_{left})^2 + x^2}}{h_p - h} \right) - \arctan\left(\frac{\sqrt{(r_0 + l_{left})^2 + x^2}}{h_p} \right) \right) \frac{R\cos\beta}{\cos^2\phi} d\phi \\ &= \int_{\beta}^{\pi} \frac{D_0 a_{1t_1} \Gamma_\delta e^{-\lambda t}}{h_F} \left(\arctan\left(\frac{\sqrt{(r_0 - R\cos\beta)^2 + (R\cos\beta\tan\phi)^2}}{h_p - h} \right) - \arctan\left(\frac{\sqrt{(r_0 - R\cos\beta)^2 + (R\cos\beta\tan\phi)^2}}{h_p} \right) \right) \frac{R\cos\beta}{\cos^2\phi} d\phi \end{aligned} \tag{16}$$

The volume integral of the left half cylinder is:

$$V_{left} = 2\int_{\frac{\pi}{2}}^{\pi} S_{(l)left} R\cos\beta d\beta \tag{17}$$

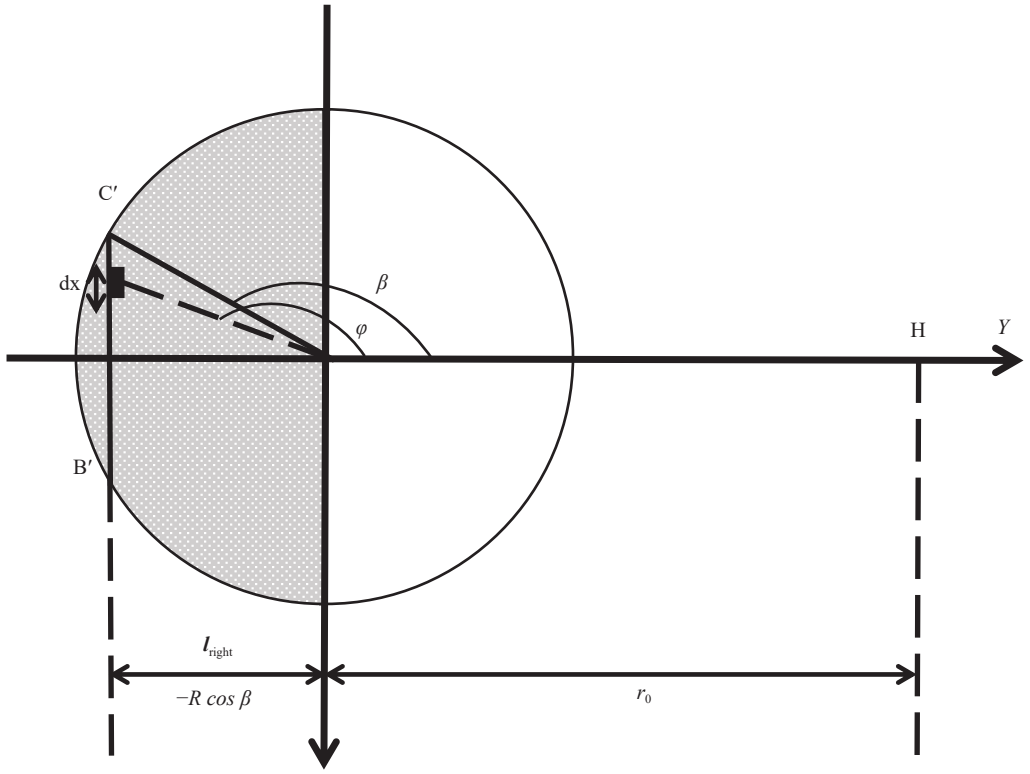

SUPPLEMENTARY FIGURE S8. Bottom view of the left half cylinder model.

Therefore, the radiation dose rate expression from the cylinder to point P is denoted as G_{left}:

$$
\begin{aligned}
G &= G_{right} + G_{left} \\
&= 2\int_0^{\frac{\pi}{2}} S_{(l)right} R\cos\beta d\beta + 2\int_{\frac{\pi}{2}}^{\pi} S_{(l)left} R\cos\beta d\beta \\
&= 2\int_0^{\frac{\pi}{2}}\int_0^{\beta} \frac{D_0 a_{1t_1}\Gamma_\delta e^{-\lambda t}}{h_F}\left(\arctan\left(\frac{\sqrt{(r_0 - R\cos\beta)^2 + (R\cos\beta\tan\phi)^2}}{h_p - h}\right)\right. \\
&\left. - \arctan\left(\frac{\sqrt{(r_0 - R\cos\beta)^2 + (R\cos\beta\tan\phi)^2}}{h_p}\right)\right)\frac{R\cos\beta}{\cos^2\phi} R\cos\beta d\phi d\beta \\
&+ 2\int_{\frac{\pi}{2}}^{\pi}\int_{\beta}^{\pi} \frac{D_0 a_{1t_1}\Gamma_\delta e^{-\lambda t}}{h_F}\left(\arctan\left(\frac{\sqrt{(r_0 - R\cos\beta)^2 + (R\cos\beta\tan\phi)^2}}{h_p - h}\right)\right. \\
&\left. - \arctan\left(\frac{\sqrt{(r_0 - R\cos\beta)^2 + (R\cos\beta\tan\phi)^2}}{h_p}\right)\right)\frac{R\cos\beta}{\cos^2\phi} R\cos\beta d\phi d\beta
\end{aligned}
\tag{18}
$$

REFERENCES

1. Luo Z. Design and implementation of a fully immersive VR training system for nuclear radiation monitoring. China Safety Science Journal 2023;33(01): 130 – 5. https://link.cnki.net/doi/10.16265/j.cnki.issn1003-3033.2023.01.0146. (In Chinese).